Effect of Parameter Identification Procedure of the Static Hysteresis Model on Dynamic Hysteresis Loop Shapes

S. Steentjes[1], M. Petrun[2], D. Dolinar[2], and K. Hameyer[1]

[1]Institute of Electrical Machines, RWTH Aachen University, Aachen D-52062, Germany
[2]Institute of Power Engineering, University of Maribor, Maribor SI-2000, Slovenia

This paper compares two different identification methods of a static rate-independent energy-based hysteresis model with regard to the dynamic hysteresis loop shape prediction when coupled to the parametric magnetodynamic lamination model. The values of hysteresis model parameters are determined solely based on the quasi-static major loop. A semiphysical approach identifying the reversible and irreversible field components independently and a purely mathematical scheme using a differential evolution optimization algorithm determining all parameters simultaneously are compared. Both variants of parameter identification are analyzed in terms of hysteresis loop shape prediction for quasi-static as well as dynamic loops.

Index Terms— **Differential evolution (DE), hysteresis modeling, magnetization dynamics, parameter identification, thermodynamics.**

I. Introduction

MODELING of magnetization dynamics, transients, and iron losses in laminated structures of nonoriented (NO) soft magnetic steel sheets (SMSSs) is a complex problem [1]. The applied hysteresis model to represent the constitutive relation of the sheet plays a central role for the resulting eddy current and flux distributions. There exists so far no macroscopic material model simultaneously considering dynamic hysteresis, the laminated structure, and the issue of parameter identification.

Initially, magnetic hysteresis loops were modeled using mathematical models, e.g., the Preisach model [2] and its descendants or the stop-and-play models [3], [4]. These models are not closely related to the physics of the magnetic materials, and rely instead on empirical techniques involving the identification of parameters. Physical-based models such as the energy-based hysteresis models involve a population of pseudoparticles with friction-like pinning [5]–[7] or the quasi-mesoscopic model that minimizes the total energy to derive a fictitious reversible and an irreversible magnetic field component [8]. Likewise, the field-separation principle advanced in [9] and [10] resembles the aforementioned descriptions of magnetic hysteresis. Those energy-based descriptions obtain the hysteresis loop branches by the introduction of an offset along the H-axis. These models are consistent with the laws of irreversible thermodynamics making those hysteresis models particularly interesting for engineers, who need reliable hysteresis models based on sound physical grounds.

This paper establishes a material model as an intermediate representation between measured data and macroscopic material characteristics. An energy-based hysteresis model, which is based on the decomposition of total field strength into reversible and irreversible terms, is presented in Section II. The values of model parameters are determined using experimental data and are expected to be more intrinsic and objective than those of empirical models, and hence better correlated with microstructure parameters. A semiphysical approach is elaborated in Section IV to identify model parameters. In comparison, a purely mathematical identification scheme minimizing the least squares error along the complete hysteresis curve using the differential evolution (DE) optimization algorithm is studied. The effect of static hysteresis model parameter identification on the models accuracy is analyzed in terms of hysteresis loop shape prediction in Section V.

Manuscript received September 7, 2015; revised December 15, 2015; accepted December 21, 2015. Date of publication January 8, 2016; date of current version April 15, 2016. Corresponding authors: S. Steentjes (e-mail: simon.steentjes@iem.rwth-aachen.de) and M. Petrun (e-mail: martin.petrun@um.si).

Color versions of one or more of the figures in this paper are available online at http://ieeexplore.ieee.org.

Digital Object Identifier 10.1109/TMAG.2015.2511800

II. Energy-Based Hysteresis Model

The energy-based hysteresis model considered in this paper is an example of the so-called *primal* or *inverse models*, i.e., time-dependent magnetic flux density $B(t)$ plays the role of an independent variable, thereby a straightforward implementation in voltage- and current-driven versions of the parametric magnetodynamic (PMD) lamination model is possible [11]–[13].

The hysteresis description is based on decoupling of the magnetic field strength in a reversible and an irreversible part consistent with the laws of thermodynamics, thereby, the source of problems originating in the assumption that total magnetization could be split into the reversible and the irreversible component is bypassed. The structure of the model enables an inclusion of dynamic eddy current effects.

The concept of anhysteretic curve (truly reversible in the thermodynamic sense) is present in the hysteresis model proposed by the GRUCAD group [9], [10]. The total field strength H is calculated from the integration of the sum of anhysteretic magnetic field H_{an} and hysteretic magnetic field H_{h} components using (1)

$$\frac{\mathrm{d}H}{\mathrm{d}t} = \frac{\mathrm{d}H_{\mathrm{an}}}{\mathrm{d}t} + \frac{\mathrm{d}H_{\mathrm{h}}}{\mathrm{d}t}. \tag{1}$$

In order to obtain a system of ODEs for direct time dependent integration, H_{an} is determined by solving (2)

$$\frac{\mathrm{d}H_{\mathrm{an}}}{\mathrm{d}B} = \frac{a_{\mathrm{an}} - \alpha_{\mathrm{an}} M_{\mathrm{ans}} \mathrm{L}'(\lambda_{\mathrm{an}})}{\mu_0 [a_{\mathrm{an}} + (1-\alpha_{\mathrm{an}}) M_{\mathrm{ans}} \mathrm{L}'(\lambda_{\mathrm{an}})]} \tag{2}$$

where λ_{an} is defined by (3) and α_{an}, a_{an}, and M_{ans} represent anhysteretic field component model parameters:

$$\lambda_{\mathrm{an}} = \frac{1}{a_{\mathrm{an}}} \left[(1-\alpha_{\mathrm{an}}) H_{\mathrm{an}} + \alpha_{\mathrm{an}} \frac{B}{\mu_0} \right]. \tag{3}$$

The ODE representing the static hysteresis component of the field is given by (4)

$$\frac{\mathrm{d}H_{\mathrm{h}}}{\mathrm{d}B} = \frac{H_{\mathrm{hs}} L(\lambda_{\mathrm{h}}) - H_{\mathrm{h}}}{\delta \gamma_{\mathrm{h}}} \tag{4}$$

where λ_{h} is defined by (5) and γ_{h}, a_{h}, and H_{hs} represent the hysteretic field component model parameters, whereas δ is the directional (control) variable that corresponds to the sign of the derivative of the magnetic flux density $\mathrm{d}B/\mathrm{d}t$:

$$\lambda_{\mathrm{h}} = \frac{1}{a_{\mathrm{h}}} [H_{\mathrm{h}} + \delta H_{\mathrm{hs}}]. \tag{5}$$

In the GRUCAD description, the well-known Langevin function L and its derivative L' are used, which are defined by (6a) and (6b)

$$\mathrm{L}(x) = \left[\coth x - \frac{1}{x} \right] \tag{6a}$$

$$\mathrm{L}'(x) = \left[1 - \coth^2 x + \left(\frac{1}{x} \right)^2 \right]. \tag{6b}$$

This *primal* inverse hysteresis description is coupled in the following to the PMD lamination model to account for the diffusion phenomena occurring under arbitrary excitations.

III. Lamination Model—PMD

When modeling magnetization dynamics in SMSSs, the static description of the material's magnetic properties is not sufficient due to high electrical conductivity of the material. This constitutive property enables the generation of unwanted eddy currents inside the SMSSs due to the alternating magnetic field. Induced eddy currents not only increase the power losses inside the SMSS but also influence the distribution of the magnetic field and consequently the shape of the dynamic hysteresis loop.

When considering NO SMSSs, the magnetic domains inside the material are small enough that the classical eddy current model is applicable, where the eddy currents are assumed to flow parallel to the surface of the SMSS and the domain dynamics are neglected [1]. At the same time, most SMSSs are thin enough that the 1-D approximation describes the diffusion phenomena with adequate accuracy [14].

In this paper, the dynamic extension is considered using the PMD model of SMSSs [11]–[13], and hence, it enables effortless implementation of different inverse static hysteresis descriptions. In the PMD, each SMSS is discretized into N slices, where the magnetic field in each slice is described with its average values. Most importantly, the distribution of induced eddy currents and their feedback on the magnetic field inside the SMSS is accounted for. The PMD can be expressed as a system of nonlinear ODEs by (7) in the form of a matrix differential equation [11], [14]

$$\boldsymbol{\Theta} = \mathbf{N} i_{\mathrm{p}} = \overline{\mathbf{H}}(\overline{\boldsymbol{\Phi}}) l_{\mathrm{m}} + \mathbf{L}_{\mathrm{m}} \frac{\mathrm{d}\overline{\boldsymbol{\Phi}}}{\mathrm{d}t} \tag{7}$$

where $\boldsymbol{\Theta}$ represents a vector of the magnetomotive forces generated by the applied current i_{p} in the excitation winding, $\mathbf{N}$ is a vector with the number of turns n_{p} of the excitation winding, $\overline{\mathbf{H}}(\overline{\boldsymbol{\Phi}})$ is a vector of average magnetic field strengths as hysteretic functions of the average magnetic fluxes in the slices, l_{m} is the magnetic path length, and $\mathbf{L}_{\mathrm{m}}$ is the so-called magnetic inductance matrix [11]–[14].

The size of the obtained ODE system depends on the discretization of the observed SMSS, i.e., the number of slices N. In the case when only one slice is used ($N = 1$), the PMD model gives the classical low-frequency eddy current approximation [14].

IV. Parameter Identification

The six parameters (α_{an}, a_{an}, M_{ans}, γ_{h}, a_{h}, and H_{hs}) of the GRUCAD hysteresis model are determined from the measurements of the static major hysteresis loop of the SMSSs using two different approaches.

The first approach is based on a semiphysical foundation where the anhysteretic and hysteretic parts of the GRUCAD model are identified separately. The anhysteretic magnetization curve is utilized to identify the reversible anhysteretic field component (parameters α_{an}, a_{an}, and M_{ans}), whereas the offsets of the ascending/descending branches along the H-axis with respect to the anhysteretic magnetic field component, i.e., the coercivity, are used to identify the irreversible hysteretic components (parameters γ_{h}, a_{h}, and H_{hs}).

The central material characteristic is the anhysteretic magnetization curve representing the thermodynamic equilibrium state of a ferromagnetic material. The anhysteretic behavior is commonly identified using the conventional field cycling method where a large alternating field of gradually decaying amplitude is applied together with a specified direct current field. The resulting magnetic flux density value defines one point on the anhysteretic magnetization curve. Repeating this, the anhysteretic magnetization curve is obtained point by point. However, uncertainties about the generality of this method remain [15].

Starting from the reversible one, the anhysteretic magnetization curve parameters α_{an}, a_{an}, and M_{ans} can be identified by least squares error minimization of the error between model prediction using (2) and (3) and the anhysteretic magnetization curve. α_{an} is the weighting factor between the reversible and irreversible parts and a_{an} affects the slope of the reversible field component (3). Once the reversible field component is identified, the offset of the ascending/descending branch of the static major loop originating from the local pinning fields hindering the domain wall motion toward thermodynamic equilibrium is attributed to the irreversible field component (4), (5). This allows identifying the parameters γ_{h}, a_{h}, and H_{hs}. H_{hs} is identified based on the behavior of the coercivity. Finally, γ_{h}, and a_{h} are identified by least squares minimization of the

error between the measured ascending branch of the measured quasi-static major hysteresis loop and the simulated ascending branch using the identified parameters describing the reversible field in (1).

The second approach is based solely on the mathematical foundation, where all six GRUCAD parameters are determined simultaneously. These parameters are determined in such a way that the minimum root-mean-square error ε between measured $B_{i\mathrm{meas}}$ and calculated flux densities $B_{i\mathrm{model}}$ for the given set of $H_{i\mathrm{meas}}$ is obtained. For this purpose, the optimization algorithm DE is applied. DE is a stochastic search algorithm suitable for finding global minimums in nonlinear and bounded optimization problems. It mimics the evolution of nature by generating populations of individuals, the properties of which are evaluated using an objective function. The individuals of the next generation are stochastically generated from individuals of the existing generation by considering the crossover probabilities and mutations according to the DE rules [16]. Only those newly generated individuals with improved objective function values survive and replace individuals of the existing generation within the next generation. In this way, the objective function values of the individuals are improved from generation to generation, which leads to the optimal solution.

The used optimization objective function is given by

$$\varepsilon = \sqrt{\sum_{i=1}^{N_\mathrm{m}} \frac{(B_{i\mathrm{meas}} - B_{i\mathrm{model}})^2}{N_\mathrm{m}}} \tag{8}$$

where N_m denotes the number of measured points of the magnetic flux density. The measured average magnetic flux density $B_{i\mathrm{meas}}$ and average magnetic field strength $H_{i\mathrm{meas}}$ in the sample were obtained using the Epstein frame within a computer-aided setup in accordance with IEC 60404-2.

In addition to the six GRUCAD parameters, also the PMD parameters are determined, where the parameters depend only on the geometric material properties and on the discretization of the observed SMSS [13], [14]. While the geometric properties (thickness, width, mean magnetic path length, and effective cross section) are determined using measurements inside relative tight tolerances [11], the measurement of the specific electric conductivity is more complicated. Hence, it can also be seen as a variable inside a prescribed interval to enhance the accuracy of the predicted results.

V. Results

The parameters of the hysteresis model were determined using both approaches solely from the major static hysteresis loop with $B_\mathrm{max} = 1.5$ T. A comparison of the obtained hysteresis model parameters is shown in Table I, whereas the measured loop and both modeled static hysteresis loops are shown in Fig. 1.

Both approaches result in different sets of parameters. Bigger deviations are visible in the parameter of the hysteretic part, whereas the anhysteretic parameters show surprisingly good agreement. However, the obtained parameters are on the same order of magnitude, which means that both the obtained

TABLE I
Identified GRUCAD Model Parameters

Par.	Quantity	Appr. 1	Appr. 2
a_an	slope of reversible field part	99.266 A/m	103.245 A/m
α_an	weight of irreversible and reversible part	$2{\cdot}10^{-4}$	$2.39{\cdot}10^{-4}$
M_ans	saturation magnetization	$1.259{\cdot}10^{6}$ A/m	$1.266{\cdot}10^{6}$ A/m
a_h	slope of irreversible field part	1.24 A/m	23.77 A/m
γ_h	shape of the irreversible part	$6.8{\cdot}10^{-3}$ A/m	$4.21{\cdot}10^{-2}$ A/m
H_hs	width of major static loop	50.09 A/m	55.47 A/m

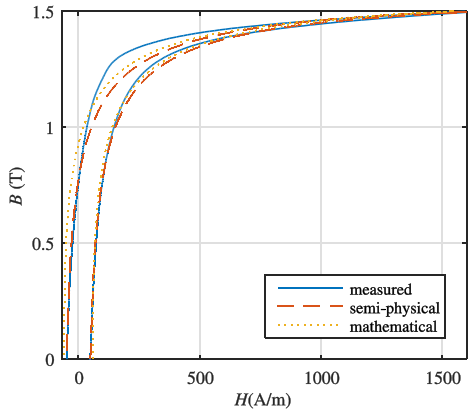

Fig. 1. Comparison of the measured static hysteresis loop with the modeled hysteresis loops determined using both discussed approaches.

sets do not deviate much from the best set of parameters. Both calculated static hysteresis loops describe the measured static loop fairly well despite some bigger deviations in different regions. The loop determined using the semiphysical approach deviated at the loop knee, whereas the loop determined using the mathematical approach described the knee region better, but at the expense of the hysteretic part. It is also very important to note that both approaches are very prone to B_max of the measured static loop and that the mathematical approach optimizes the deviations based on the whole loop in one step in contrast to the two-step semiphysical approach. Problems arise when the model parameter is identified based on major loops that have B_max deep in saturation. It is almost impossible to obtain a set of parameters that describe both regions (hysteretic and saturation) of the static hysteresis with good accuracy. Possible reason for the present limitation of the model or identification is, in particular, the suitability of the Langevin function for description of the anhysteretic magnetization curve of SMSSs [17].

Further, it was analyzed how the errors of the modeled static hysteresis loops influence the dynamic behavior using the PMD model. Fig. 2 shows the comparison of dynamic hysteresis loops at 50 Hz (first row), 100 Hz (second row), 400 Hz (third row), and 1000 Hz (fourth row) for sinusoidal voltage excitation. The first column shows dynamic loops at $B_\mathrm{max} = 1$ T, whereas the second column at $B_\mathrm{max} = 1.5$ T. It is apparent that the semiphysical approach leads to more accurate results than the purely mathematical one,

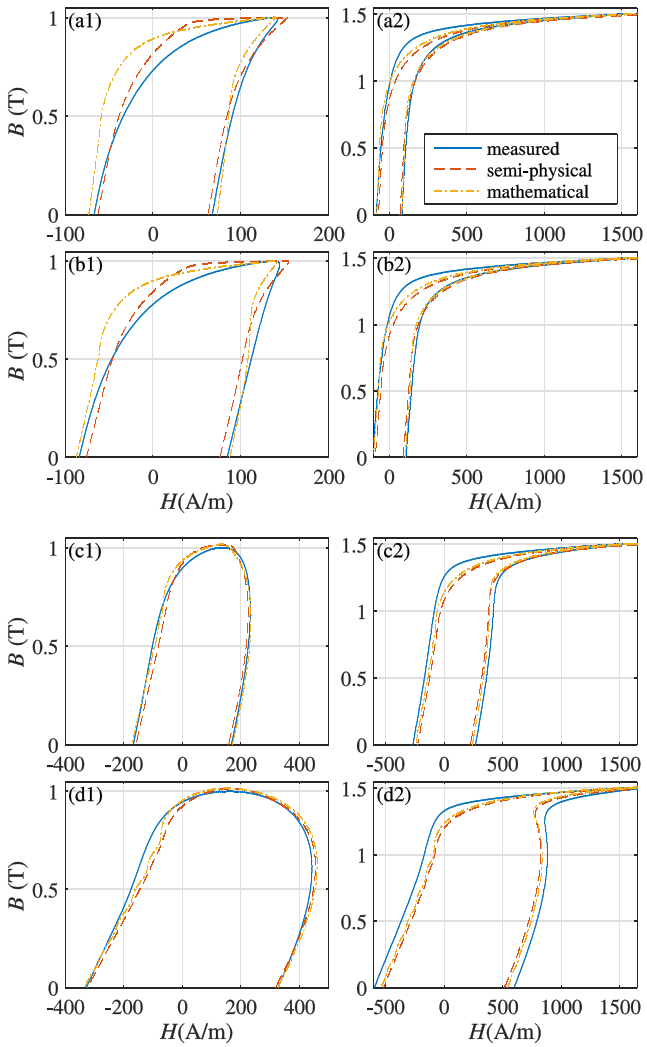

Fig. 2. Comparison of the measured and calculated dynamic hysteresis loops. First row: $f = 50$ Hz. Second row: $f = 100$ Hz. Third row: $f = 400$ Hz. Fourth row: $f = 1000$ Hz. First column: $B_{\max} = 1$ T. Second column: $B_{\max} = 1.5$ T.

supporting the related parameter set. Deviations around the knee are still apparent but less significant at higher frequencies.

VI. Conclusion

This paper discussed the integration of an energy-based hysteresis model into the PMD model and its parameter identification based on two different methods solely using the quasi-static major loop. The results of modeling symmetric minor loops at various frequencies using the major loop parameters in combination with the PMD are in good agreement with the experimental data. Inaccuracies are obtained around the knee of the hysteresis loops, which can be attributed to the usage of the Langevin function. Future work will focus on extension of the reversible field component to account for the magnetization behavior in both the domain wall motion and rotation areas, respectively.

Acknowledgment

The work of M. Petrun and D. Dolinar was supported in part by ARRS under Project P2 0115, Project L2 5489, and Project L2 4114. The work of S. Steentjes was supported in part by German Research Foundation (DFG) and carried out in the research project Improved Modeling and Characterization of Ferromagnetic Materials and Their Losses.

References

[1] S. E. Zirka *et al.*, "Dynamic magnetization models for soft ferromagnetic materials with coarse and fine domain structures," *J. Magn. Magn. Mater.*, vol. 394, pp. 229–236, Nov. 2015.

[2] S. Bi, F. Wolf, R. Lerch, and A. Sutor, "An inverted Preisach model with analytical weight function and its numerical discrete formulation," *IEEE Trans. Magn.*, vol. 50, no. 11, Nov. 2014, Art. ID 7300904.

[3] T. Matsuo and M. Shimasaki, "Two types of isotropic vector play models and their rotational hysteresis losses," *IEEE Trans. Magn.*, vol. 44, no. 6, pp. 898–901, Jun. 2008.

[4] T. Matsuo, D. Shimode, Y. Terada, and M. Shimasaki, "Application of stop and play models to the representation of magnetic characteristics of silicon steel sheet," *IEEE Trans. Magn.*, vol. 39, no. 3, pp. 1361–1364, May 2003.

[5] A. Bergqvist, "Magnetic vector hysteresis model with dry friction-like pinning," *Phys. B, Condens. Matter*, vol. 233, no. 4, pp. 342–347, 1997.

[6] F. Henrotte and K. Hameyer, "A dynamical vector hysteresis model based on an energy approach," *IEEE Trans. Magn.*, vol. 42, no. 4, pp. 899–902, Apr. 2006.

[7] S. Steentjes, F. Henrotte, C. Geuzaine, and K. Hameyer, "A dynamical energy-based hysteresis model for iron loss calculation in laminated cores," *Int. J. Numer. Model, Electron. Netw., Device, Fields*, vol. 27, no. 3, pp. 433–443, 2013.

[8] H. Hauser, "Energetic model of ferromagnetic hysteresis: Isotropic magnetization," *J. Appl. Phys.*, vol. 96, no. 5, pp. 2753–2767, 2004.

[9] P. Koltermann, L. A. Righi, J. P. A. Bastos, R. Carlson, N. Sadowski, and H. J. Batistela, "A modified Jiles method for hysteresis computation including minor loops," *Phys. B, Condens. Matter*, vol. 275, nos. 1–4, pp. 233–237, 2000.

[10] P. Koltermann *et al.*, "Nonlinear magnetic field model by FEM taking into account hysteresis characteristics with M-B variables," *IEEE Trans. Magn.*, vol. 38, no. 2, pp. 897–900, Mar. 2002.

[11] M. Petrun, V. Podlogar, S. Steentjes, K. Hameyer, and D. Dolinar, "A parametric magneto-dynamic model of soft magnetic steel sheets," *IEEE Trans. Magn.*, vol. 50, no. 4, Apr. 2014, Art. ID 7300304.

[12] M. Petrun, V. Podlogar, S. Steentjes, K. Hameyer, and D. Dolinar, "Power loss calculation using the parametric magneto-dynamic model of soft magnetic steel sheets," *IEEE Trans. Magn.*, vol. 50, no. 11, Nov. 2014, Art. ID 6301304.

[13] M. Petrun, S. Steentjes, K. Hameyer, and D. Dolinar, "Magnetization dynamics and power loss calculation in NO soft magnetic steel sheets under arbitrary excitation," *IEEE Trans. Magn.*, vol. 51, no. 1, Jan. 2015, Art. ID 7300104.

[14] M. Petrun, S. Steentjes, K. Hameyer, and D. Dolinar, "One-dimensional lamination models for calculating the magnetization dynamics in non-oriented soft magnetic steel," *IEEE Trans. Magn.*, DOI: 10.1109/TMAG.2015.2480416, to be published.

[15] J. Pearson, P. T. Squire, and D. Atkinson, "Which anhysteretic magnetization curve?" *IEEE Trans. Magn.*, vol. 33, no. 5, pp. 3970–3972, Sep. 1997.

[16] K. V. Price, R. V. Storn, and J. A. Lampinen, *Differential Evolution: A Practical Approach to Global Optimization*. New York, NY, USA: Springer, 2005.

[17] M. W. Gutowski and E. Kokornaczyk, "Anhysteretic functions for the Jiles–Atherton model," *IEEE Trans. Magn.*, vol. 51, no. 2, Mar. 2015, Art. ID 7300305.